OVRO-LWA Memo No. 17

Cable Reflections in Stage 3 Autocorrelation Delay Spectra

Katherine Elder
Arizona State University

2025 August 6

Submitted 2025 August 6

To cite this memo in another document, use:
"OVRO-LWA Memo 17, 2025 Aug 6, http://tauceti.caltech.edu/LWA/lwamemos.html "

Cable Reflections in Stage 3 Autocorrelation Delay Spectra

Katherine Elder

August 2025

1 Introduction

Stage II of the OVRO-LWA consisted of 256 dual-polarization dipole antennas with a maximum baseline of 1.5 km (Anderson et al., 2019). Stage III upgrades began in 2020 to expand the array to 352 antennas with a maximum baseline of 2.4 km (Hallinan et al., 2023). A known concern from the Stage II array was the presence of cable reflections. Reflections occur when some portion of the signal is reflected along the cable to the antenna feed, where it is reflected again and travels back to the analog receiver (ARX) board. Reflections can be caused by defects in the cable or errors at the SMA connector, either a faulty connection or an impedance mismatch. These reflections will appear in the observations as a modulated copy of the signal added at a higher delay. This can contaminate the region of the spectrum where the 21 cm signal is expected to be detectable (O'Hara et al., 2024). Part of the Stage III upgrade included the development of improved Analog Receiver (ARX) boards. The goal was for cable reflections to be reduced with the upgraded ARX boards and therefore increase the chances of detecting the 21 cm signal.

Delay spectra are commonly used to identify non-astrophysical sources of spectral structure in observations (Kolopanis et al., 2023). The delay spectrum is the Fourier transform along frequency to convert to time. Galactic foregrounds will be constrained to low delay modes because they are spectrally smooth and evolve slowly. The 21 cm signal fluctuates quickly and will be detectable at higher delay models. Uncorrected structure in the observations, such as cable reflections, contaminates these higher delay modes (Pober et al., 2013). To test whether a feature in the data is caused by cable reflections, the delay can be used to calculate the extra distance the signal traveled. This distance is then compared to the list of cable lengths provided by the on-site staff to see how well the distances match. The 21 cm signal is expected to

be $\sim$ 60 dB below the total foreground power during the Cosmic Dawn and thus instrumental structure in the bandpass must be suppressed to 70 dB below the foreground power (Trott et al., 2020).

Early OVRO-LWA science results placed constraints on the 21 cm global signal (Price et al., 2018), as well as constraints on the angular 21 cm power spectrum (Eastwood et al., 2018, 2019). Garsden et al. (2021) used data from Stage II to measure the 21 cm power spectrum at 48 MHz. In the results, they note that cable reflections have been reported by other power spectra experiments, such as Beardsley et al. (2016), and are a possible limiting factor in the OVRO-LWA as well. Bowman (2019) provided an overview of cable reflections in the Stage II array and provided suggested requirements for the Stage III array to eliminate cable reflections as a limiting factor. This memo follows up on Bowman (2019) and studies the presence of cable reflections in the Stage III array.

2 Cable Reflections

Buried coaxial cables connect the core antennas to the backend system, which is located in a shelter near the telescope core. The cables vary in length from $\sim$35-450 m outside of the shelter and then are connected to $\sim$10 m cables inside the shelter which connect to the ARX boards. Cable reflections can be caused by a number of factors, most commonly impedance mismatch at the SMA connector between the cables and the ARX board (Kern et al., 2019). This causes the signal to reflect back to the antenna feed, where it is reflected a second time at the antenna before entering the ARX board. This double reflection produces a characteristic frequency ripple in the antenna gain which corresponds to a distance of 2$\times$ the cable length. The structure caused by the reflection will convolve with foregrounds and cause contamination in the spectrum.

A useful tool to examine bandpass spectral structure is to use the delay spectrum of the autocorrelations. Autocorrelations are the cross-correlation of an antenna with itself. This produces a spectrum which approximates the bandpass of the telescope. The delay spectrum is the square of the absolute value of the Fourier transform along frequency. For 21 cm cosmology, the delay spectrum maps to the line-of-sight for the telescope. This constrains the bright galactic foregrounds to low delay modes and the 21 cm signal to higher delays. Foregrounds are spectrally smooth and evolve slowly, while the 21 cm signal has spectral structure and has quick fluctuations. Cable reflections appear as attenuated copies of the foregrounds at higher delays, which can mimic the appearance of the 21 cm signal (O'Hara et al., 2024).

Due to variations in the hardware and cable length, cable reflections are not uniform across all antennas. Additionally, not all antennas experience noticeable cable reflections, or the same amplitude of reflection. It is therefore difficult to create a model of cable reflections which can be applied equally to the entire array. Instead, a crude algorithm is used on an antenna-by-antenna basis to identify the brightest source beyond the foregrounds in the delay spectrum. This delay is then used to calculate the corresponding cable length the signal would have traveled using the following equation:

$$L = \frac{\nu_c \tau}{2} \tag{1}$$

where L is the cable length in meters, ν_c is the wave propagation speed in the cable, and τ is the delay in nanoseconds. The OVRO-LWA uses LMR 240 cables, supplied by Burns Industries, which have $\nu_c = 0.84c$. This value can be plugged into Eqn. 1:

$$L \sim 0.126\tau \tag{2}$$

The cable length calculated from the delay spectrum is then compared to the cable length of the given antenna. The cable lengths for each antenna were provided by the OVRO staff. The amplitude of the cable reflection is then used to set the dynamic range, which is the ratio between the peak foreground power and the power of the assumed cable reflection.

Some restrictions are needed in order to determine if the identified feature is actually a cable reflection. The simplest method is to use the noise floor. The noise floor is calculated by taking the median of the delay spectrum beyond the foreground dominated delays. If the amplitude of the supposed cable reflection is below the noise floor, it is discarded.

2.1 Stage II data

Bowman (2019) investigated cable reflections in uncalibrated Stage II autocorrelations and the analysis has been recreated in this section. The data used was 1-second autocorrelation spectra from all 512 antenna inputs in the Stage II OVRO-LWA telescope, acquired on 04-Apr-2019 19:17:17. Data were provided by L. D'Addario on 6/18/2019. The data were limited to the sub-band ranging from 40-80 MHz due to RFI in the FM band (>87 MHz) and the ionosphere band (<20 MHz). This is also the sub-band of interest for

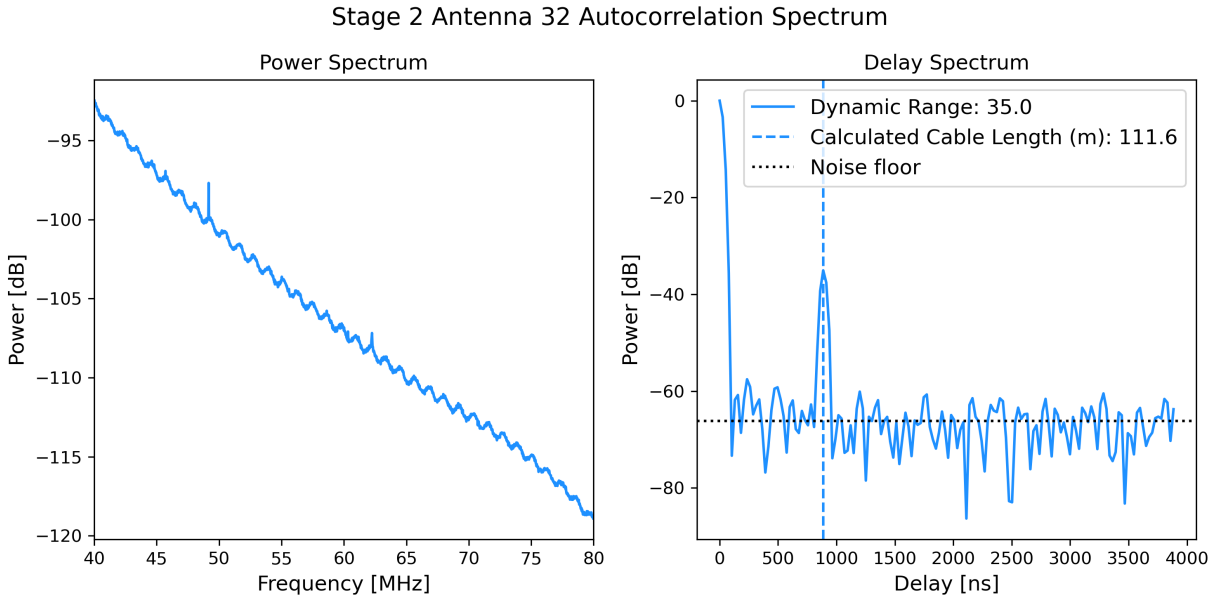

Figure 1: Autocorrelation of a single antenna 32. (Left) the power spectrum with a clear ripple present, likely caused by a cable reflection. (Right) the delay spectrum with a large peak at $\tau = 0$ ns due to foreground power. The second peak at $\sim \tau = 880$ ns is assumed to be a cable reflection. The dynamic range is 35 dB.

21 cm cosmology. A median filter was then applied using a 20-channel box to eliminate narrow band RFI in the data.

It is necessary to use a Blackman-Harris window function during the Fast Fourier Transform (FFT) to calculate the delay spectrum. This reduces the sidelobes in the spectrum, but does reduce the delay channel resolution as well as correlate neighboring channels. The power spectrum is calculated by squaring the absolute value of the resulting spectrum.

After a general quality check to ensure the antenna was operating correctly, there are 223 antennas left in the data set. Then the amplitude of the signal was checked to see if it was below the noise floor. After discarding these antennas, only 178 antennas remained.

Figure 1 is an example of an individual antenna autocorrelation from the Stage II array. The left panel is the autocorrelation with a clear ripple present. The right panel is the delay spectrum. The peak at $\tau = 0$ ns is due to the foreground power. The second prominent peak at $\sim \tau = 880$ ns is the source of the ripple in

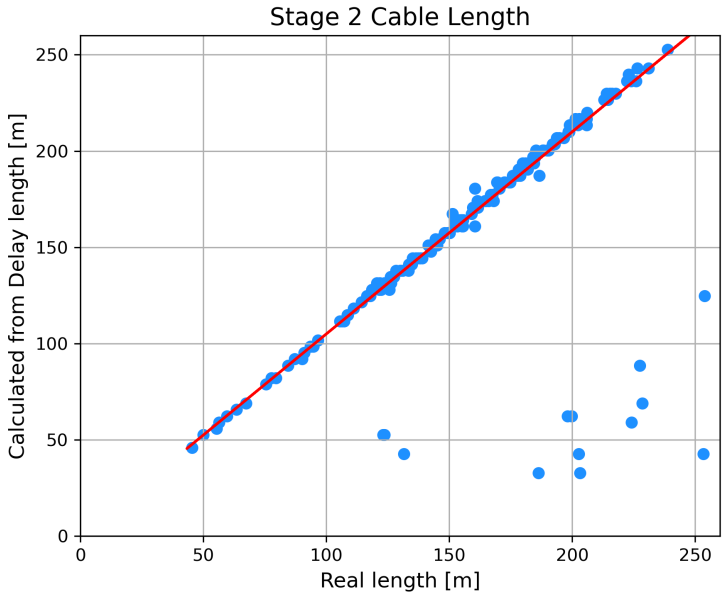

Figure 2: Comparison of the estimated cable lengths calculated from the delay spectrum to the actual measured cable lengths. Most of the antennas fall along the ideal linear line plotted in red. The outlier antennas are likely caused by some other structure present which did not correspond to a cable reflection.

the power spectrum. Using Eqn. 2, this corresponds to a length of 111.6 meters. The real length provided by the OVRO staff is 106.4 m. This secondary peak sets the limiting dynamic range at 35 dB.

Figure 2 compares the estimated cable lengths calculated from the delay spectrum to the cable lengths provided by OVRO staff. Nearly all the antennas fall along an ideal linear line, plotted in red. The outlier antennas are likely caused by some other structure creating a peak which did not correspond to a cable reflection. The origin of this peak is unknown.

2.2 Stage III data

The same analysis was completed for uncalibrated Stage III autocorrelations. The data used was 1-second autocorrelations from all 256 antenna inputs, acquired on 12-14-2022 06:00:21.

After a general quality check to ensure the antenna was operating correctly, there are 239 antennas left in the data set. Then the amplitude of the signal was checked to see if it was below the noise floor. After discarding these antennas, 196 antennas remained.

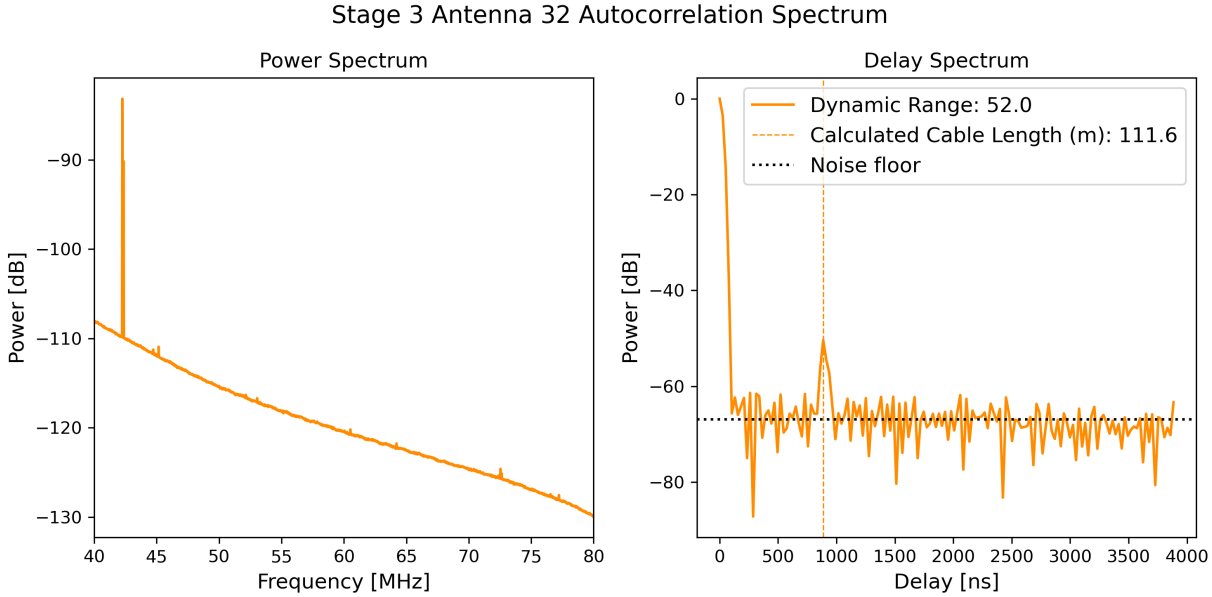

Figure 3: Autocorrelation of Antenna 32 from Stage III. (Left) the autocorrelation spectrum. There is no clear ripple like the one noted in the Stage II data. (Right) the delay spectrum with a large peak at $\tau = 0$ ns due to foreground power. The second peak at $\sim \tau = 880$ ns is assumed to be a cable reflection. The dynamic range is 52 dB.

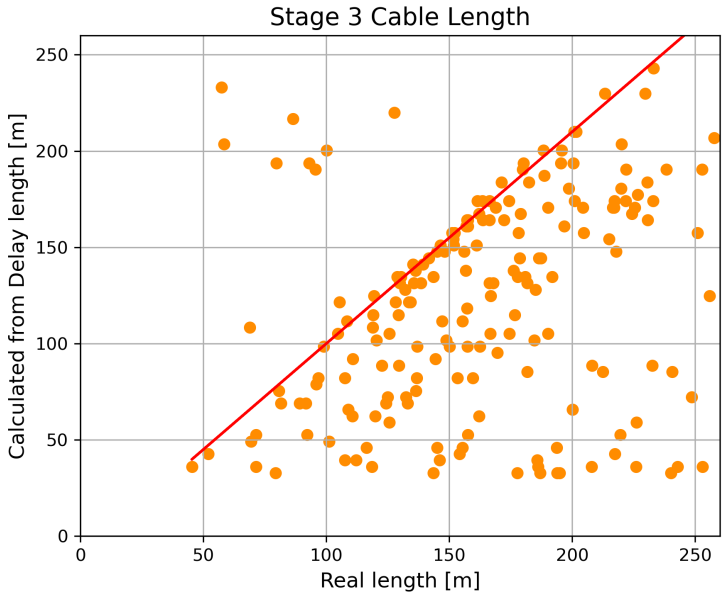

Figure 4: Comparison of the estimated cable lengths calculated from the delay spectrum to the actual measured cable lengths. While some of the antennas fall along the ideal linear line plotted in red, most do not. The outlier antennas are likely due to some other structure present which did not correspond to a cable reflection.

Figure 3 is an example of an individual antenna autocorrelation from the Stage III array, using the same antenna as in Figure 1. The left panel is the autocorrelation spectrum. There is no clear ripple present as there was in the Stage II data. The right panel is the delay spectrum. The presumed cable reflection appears at $\sim \tau = 880$ ns, or 111 m. This gives a dynamic range of 52 dB.

Figure 4 is the comparison of estimated cable length calculated from the delay spectrum to the measured cable lengths which were provided by the OVRO staff. While some of the antennas fall along the ideal fit line, most do not. This could be due to some other source of structure present which did not correspond to a cable length.

To further investigate the source of these outliers, Figure 5 shows the amplitude of the supposed cable reflection plotted against the noise floor. There are a number of points which indicate the amplitude was just higher than the noise floor, causing it to be missed while filtering out antennas. This indicates that at least some of the outliers noted in the previous figure are likely caused by noise and are not real spectral

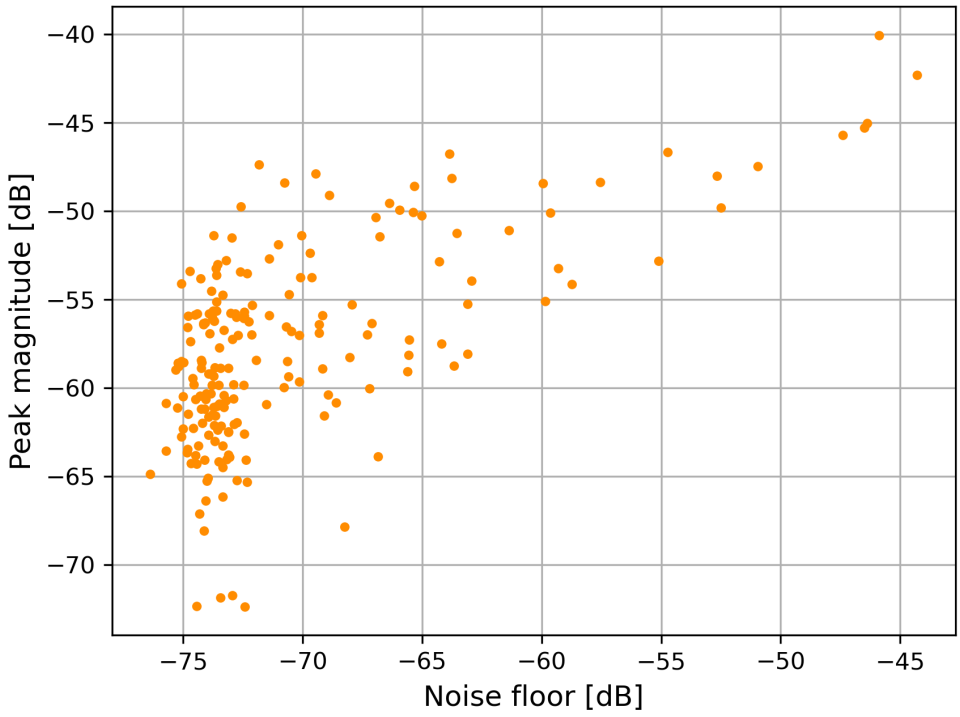

Figure 5: Comparison of the amplitude of the supposed cable reflection with the noise floor. There appear to be a number of antennas which have peaks barely above the noise floor. These likely correspond to outlier antennas noted in Figure 4

features.

2.3 Comparison and Discussion

In order to compare the two data sets, only the antennas that were in both data sets after filtering were analyzed. This left 150 antennas in the final data set.

Figure 6 compares the delay spectrum of Antenna 32 in both the Stage II and Stage III array. The antenna has an identified cable reflection in the same location for both stages. This implies that the source of the cable reflection was not altered by the upgrade to the telescope. In Stage II, the amplitude of the cable reflection limits the dynamic range to 35 dB. In Stage III, the dynamic range is 52 dB, a nearly 20 dB improvement.

Figure 7 provides a histogram of the dynamic range for the 150 antennas used in the Stage II and Stage

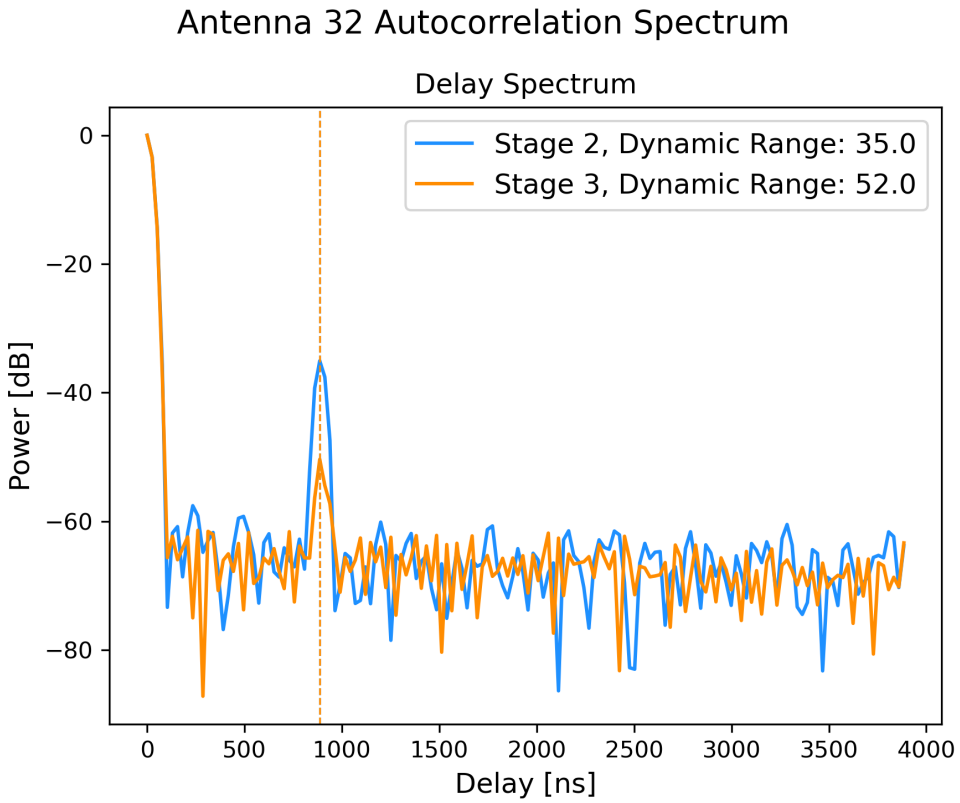

Figure 6: Comparison of the delay spectrum for antenna 32 from Stage II and Stage III. The identified cable reflection is in the same location for both data sets. In Stage II, the amplitude of the cable reflection limits the dynamic range to 35 dB. In Stage III, the dynamic range is 52 dB, a nearly 20 dB improvement.

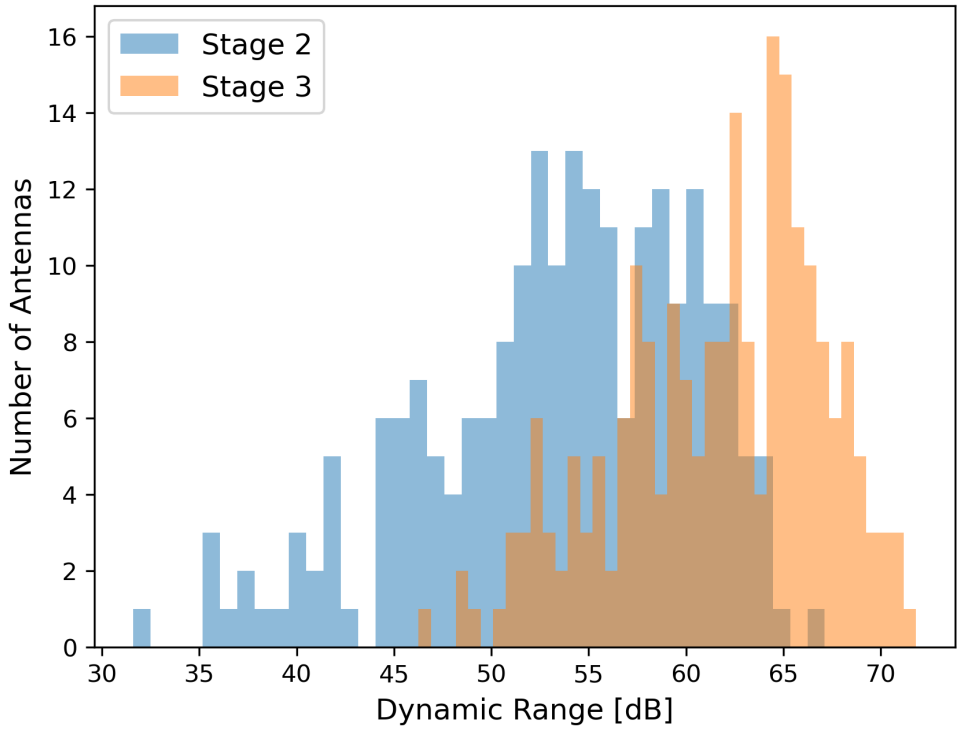

Figure 7: A histogram of the dynamic range for the 150 antennas used in the Stage II and Stage III analysis. It is clear that Stage III has improved on the dynamic range, ranging from 46-72 dB while Stage II ranges from 32-65 dB. Additionally, Stage III has more antennas at the higher end of the dynamic range than Stage II.

Metric	Stage II	Stage III
Number of Cable Refl.	132	63
% Antennas with Cable Refl.	88	42
Median Dynamic Range	52 dB	62 dB
Median Noise Floor	-63 dB	-73 dB

Table 1: A summary of the results of the cable reflection analysis. These numbers are based on the collection of 150 antennas available in both stages.

III analysis. It is clear that Stage III has improved on the dynamic range, ranging from 46-72 dB while Stage II ranges from 32-65 dB. Additionally, Stage III has more antennas at the higher end of the dynamic range than Stage II.

Before giving a final comparison of the two stages to determine how much the upgrade improved upon the cable reflections, one last restriction will be placed upon the data. Both stages identified bright peaks in the delay spectrum which were higher than the noise floor. However not all of those peaks corresponded to a cable length, particularly in the Stage III data. In some cases, it may be that there was damage to the cable which resulted in a reflection which did not travel the full length of the cable. In others, it may be that the signal only reflected within the $\sim$ 10 m cable in the shelter which connects the antenna cable to the ARX board. In that case, the signal would only add an additional $15 - 25$ m, depending on the true length of the cable. And lastly, this peak may not be caused by a cable reflection at all and is caused by some unknown source. In order to place a tight restriction on what is determined to be a cable reflection, only those peaks which correspond to a cable length within 25 m of the true cable length will be compared.

Table 1 provides a summary of the of the results from both Stage II and Stage III using these restrictions. Out of 150 antennas compared, Stage II had 132 antennas with cable reflections meaning 88% of antennas experienced cable reflections. Stage III had 63 antennas with cable reflections, meaning 42% of antennas experienced cable reflections. This is a reduction of 46% post upgrade. In Stage II, the median dynamic range for antennas with cable reflections was 52 dB while in Stage III, it is 62 dB. This is a 10 dB increase.

The original goal was to suppress instrumental structure to 70 dB in dynamic range. At the time of this analysis, cable reflections need to be reduced by an additional $\sim$ 10 dB. However, despite not meeting this crude requirement, significantly fewer antennas experience cable reflections in Stage III than in Stage

II, which was a goal of the upgrade.

3 Multi-day comparison

Identifying cable reflections is important to be able to mitigate the effects. However, the array is not in an isolated, controlled environment. This means that various outside effects can cause fluctuations in the data. These fluctuations contribute to the difficulty in creating a model of cable reflections to be used for data corrections. It is therefore of interest to identify any consistent patterns in the sources of cable reflection fluctuations which can then be modeled. Here, an analysis with a focus on temperature and is presented.

3.1 Data

1-second autocorrelations were collected at 5 AM on consecutive days from January 28-31, 2023, and from May 28-31, 2023. Table 2 lists the weather conditions in Bishop, CA for each day according to Weather Underground.[1] It is important to note that the local sidereal time (LST) at 5 AM is different in January versus May. This can affect the strength of the foregrounds based on what sources are visible at that time. However, the reason for choosing the same time for both months of observations is because 5 AM has been noted to be one of the quietest times of day for RFI and produce the smoothest power spectra. Therefore the concerns regarding observing at different LSTs has been disregarded in favor of higher quality data.

The data was processed using the same steps as in Section 2. During this analysis process, the observation from May 30th was discarded due to low quality.

3.2 Results and Discussion

Figure 8 provides an example of the autocorrelation delay spectrum of a single antenna, Antenna 6, over a total of 7 days. The vertical lines indicate where potential cable reflections were found for each day. While four of the seven days identified the possible cable reflection near the true cable length at $\sim \tau = 1770$ ns, or 223 m, three days did not. This indicates that the cable reflection was not the brightest feature consistently across all the days. The amplitude of the cable reflection fluctuates between -60 dB and -75 dB over the course of the recorded days.

[1] https://www.wunderground.com

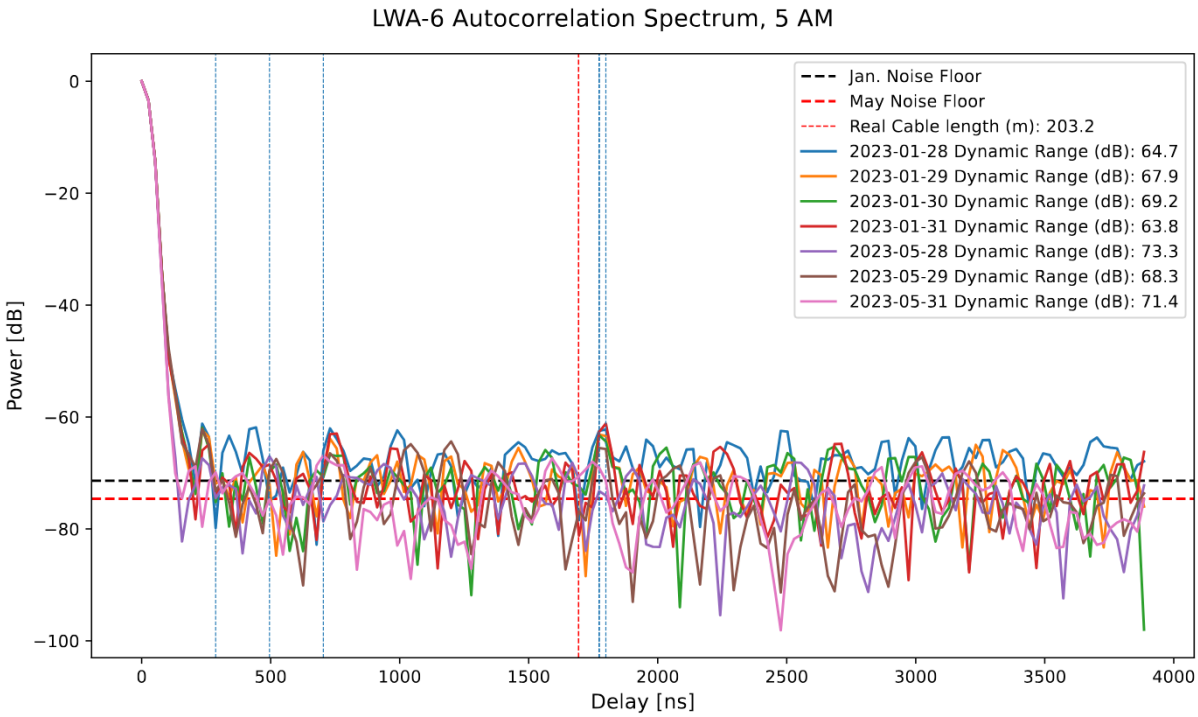

Figure 8: A comparison of the delay spectrum for antenna 6 over a total of 7 days. The various vertical lines indicate potential cable reflections. The red vertical line correspond to the true cable length. The black and red horizontal lines are the median noise floor for the antenna in January and in May. While four of the seven days identified a possible cable reflection near the true cable length, three days did not. This indicates that the cable reflection was not the brightest feature consistently across all the days.

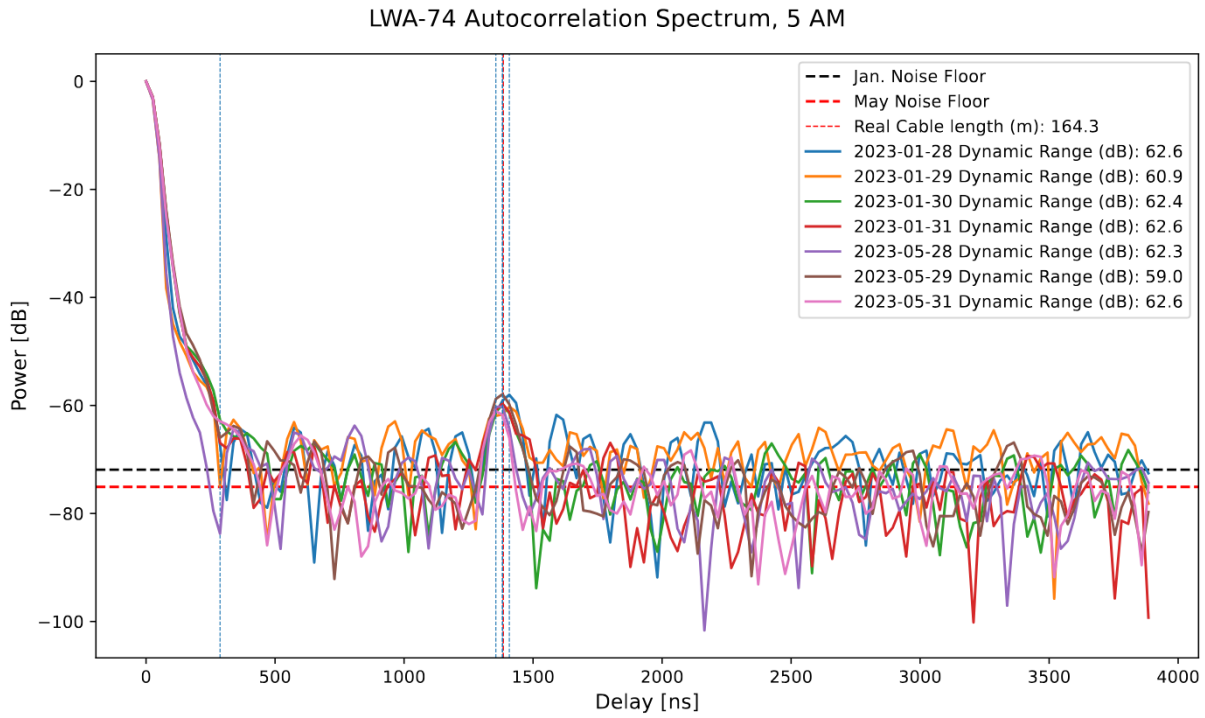

Figure 9: A comparison of the delay spectrum for antenna 74 over a total of 7 days. The vertical lines indicate potential cable reflections and are all located near the same point. The red vertical line correspond to the true cable length. The black and red horizontal lines are the median noise floor for the antenna in January and in May. All 7 days identified a prominent cable reflection.

Date	Temp. (C°)	High Temp.(C°)	Low Temp.(C°)
1/28/2023	1	11	-4
1/29/2023	-6	9	-7
1/30/2023	-1	3	-4
1/31/2023	-10	9	-10
5/28/2023	12	29	10
5/29/2023	13	29	11
5/30/2023	9	28	8
5/31/2023	12	28	11

Table 2: The historical weather conditions for Bishop, CA according to Weather Underground. The Temperature is recorded for 5 AM.

Figure 9 provides an example an autocorrelation delay spectrum with a prominent cable reflection present all 7 days. The cable reflection is near the true cable length at $\sim \tau = 1385$ ns, or 164 m. While the amplitude of the cable reflection appears very similar for all the days, it does fluctuate between -58 dB and -61 dB.

In order to properly study the change in cable reflections, the same rubric as was used in Section 2 was applied to each day of data. A general quality check revealed 241 antennas were operational in January, and 300-302 were operational in May. Next, only antennas which had peaks above the noise floor and calculated cable lengths within 25 m of the real cable length were kept for each day.

The results for the final collection of antennas is summarized in Table 3. In January, there were between 61-71 antennas with cable reflections, or 25-29% of antennas experienced cable reflections. In May, 75-84 antennas had cable reflections, or 25-28%. The noise floor decreased by $\sim 7 - 9$ dB in May, and the dynamic range increased by $\sim 1 - 5$ dB in May.

Figure 10 provides a histogram of the dynamic range for the antennas with cable reflections across 7 days. There is no noticeable pattern as the days are generally overlapping each other. There are notable spikes from January 31st, May 29th, and May 31st, but even these spikes are not dramatically different from the rest of the data.

Figure 11 plots the temperature at the time of observation for each of the 7 days vs the median dynamic

Date	#Cable Refl.	Median Noise Floor	Median Dynamic Range
1/28/2023	69	-66 dB	60 dB
1/29/2023	71	-67 dB	60 dB
1/30/2023	61	-67 dB	59 dB
1/31/2023	63	-68 dB	59 dB
5/28/2023	77	-75 dB	63 dB
5/29/2023	84	-75 dB	61 dB
5/31/2023	75	-75 dB	64 dB

Table 3: A summary of the results of the multi-day cable reflection analysis. In January, there were 241 antenna operational. In May, there were 300-302 antenna.

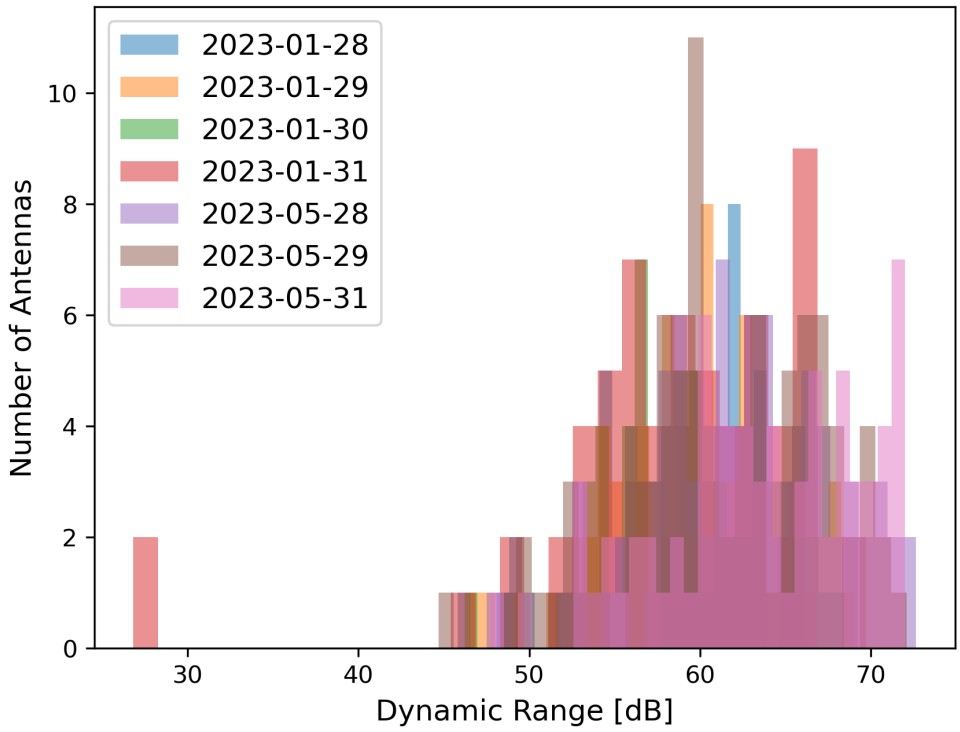

Figure 10: A histogram of the dynamic range for the antennas with cable reflections across 7 days. There is no noticeable pattern as the days are generally overlapping each other.

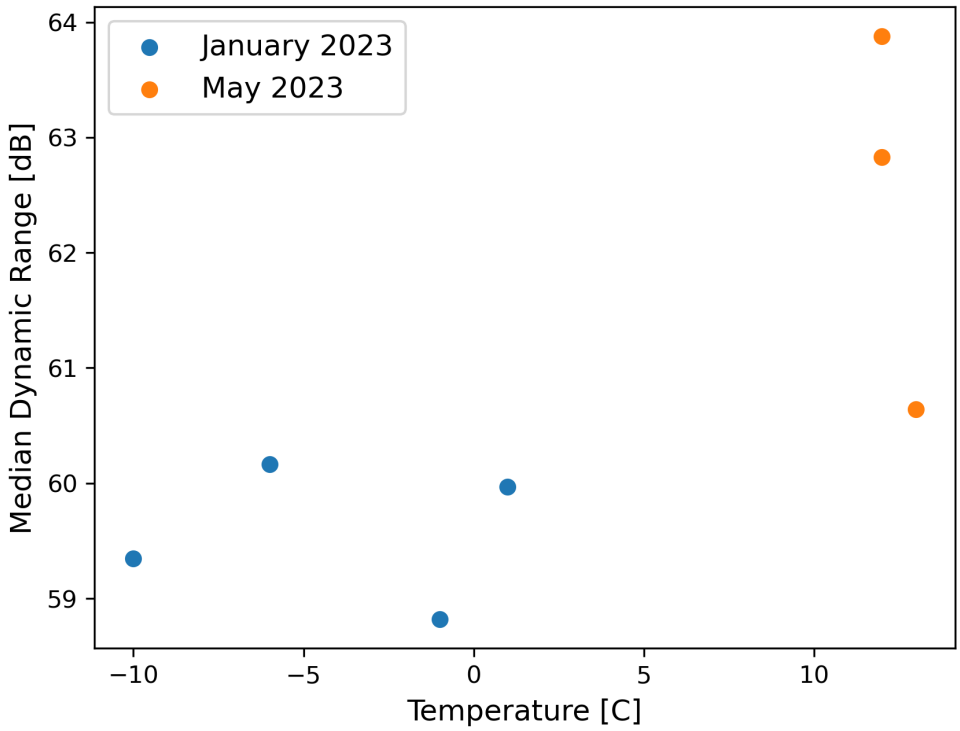

Figure 11: The temperature at the time of observation vs the median dynamic range for each day.

range. While the dynamic range is higher in May, when the temperature was higher, there is no noticeable pattern relating the dynamic range to temperature. However, with only 7 days of data, it is difficult to draw any definitive conclusions.

4 Conclusion

Cable reflections convolve galactic foregrounds to other regions of the OVRO-LWA spectrum, which can obscure the Epoch of Reionization 21 cm signal. During the Stage II OVRO-LWA, Bowman (2019) analyzed the number of cable reflections present in the array and how much they limited the ability to detect the 21 cm signal. It was estimated that to reach the requirement of a 70 dynamic range, cable reflections needed to be suppressed by an additional 30 dB.

A duplicate analysis was performed on observations from the Stage III array to quantify how much the upgrade was able to suppress cable reflections. The results of this analysis show that for the 150 antennas analyzed, there was a ~46% reduction in the amount of cable reflections present in the array post upgrade. However, the median dynamic range was only improved by 10 dB. Therefore cable reflections must be suppressed by an additional 10 dB to meet the crude 21 cm requirement.

An additional analysis was performed on multiple days of observations from the Stage III array. Consecutive days from January 2023 and May 2023 were compared to study if temperature has a consistent affect on how the amplitude of cable reflections fluctuates. If there is a direct correlation between temperature and amplitude, this effect can be modeled and used in data corrections. The results indicate that dynamic range most likely is not directly related to temperature. However, only 7 days of data was used, which is not enough to form a definitive conclusion. Further investigation with more days will be necessary to identify if there is a true relationship.

References

Anderson Marin M., Hallinan Gregg, Eastwood Michael W., Monroe Ryan M., Callister Thomas A., Dowell Jayce, Hicks Brian, Huang Yuping, Kassim Namir E., Kocz Jonathon, Lazio T. Joseph W., Price Danny C., Schinzel Frank K., Taylor Greg B. New Limits on the Low-frequency Radio Transient Sky Using 31 hr of All-sky Data with the OVRO-LWA // . XII 2019. 886, 2. 123.

Beardsley A. P., Hazelton B. J., Sullivan I. S., Carroll P., Barry N., Rahimi M., Pindor B., Trott C. M., Line J., Jacobs Daniel C., Morales M. F., Pober J. C., Bernardi G., Bowman Judd D., Busch M. P., Briggs F., Cappallo R. J., Corey B. E., de Oliveira-Costa A., Dillon Joshua S., Emrich D., Ewall-Wice A., Feng L., Gaensler B. M., Goeke R., Greenhill L. J., Hewitt J. N., Hurley-Walker N., Johnston-Hollitt M., Kaplan D. L., Kasper J. C., Kim H. S., Kratzenberg E., Lenc E., Loeb A., Lonsdale C. J., Lynch M. J., McKinley B., McWhirter S. R., Mitchell D. A., Morgan E., Neben A. R., Thyagarajan Nithyanandan, Oberoi D., Offringa A. R., Ord S. M., Paul S., Prabu T., Procopio P., Riding J., Rogers A. E. E., Roshi A., Udaya Shankar N., Sethi Shiv K., Srivani K. S., Subrahmanyan R., Tegmark M., Tingay S. J., Waterson M., Wayth R. B., Webster R. L., Whitney A. R., Williams A., Williams C. L., Wu C., Wyithe J. S. B. First Season MWA EoR Power spectrum Results at Redshift 7 // . XII 2016. 833, 1. 102.

Bowman Judd. Cable Reflections in Autocorrelation Delay Spectra OVRO-LWA REPORT. 2019.

Eastwood Michael W., Anderson Marin M., Monroe Ryan M., Hallinan Gregg, Barsdell Benjamin R., Bourke Stephen A., Clark M. A., Ellingson Steven W., Dowell Jayce, Garsden Hugh, Greenhill Lincoln J., Hartman Jacob M., Kocz Jonathon, Lazio T. Joseph W., Price Danny C., Schinzel Frank K., Taylor Gregory B., Vedantham Harish K., Wang Yuankun, Woody David P. The Radio Sky at Meter Wavelengths: m-mode Analysis Imaging with the OVRO-LWA // . VII 2018. 156, 1. 32.

Eastwood Michael W., Anderson Marin M., Monroe Ryan M., Hallinan Gregg, Catha Morgan, Dowell Jayce, Garsden Hugh, Greenhill Lincoln J., Hicks Brian C., Kocz Jonathon, Price Danny C., Schinzel Frank K., Vedantham Harish, Wang Yuankun. The 21 cm Power Spectrum from the Cosmic Dawn: First Results from the OVRO-LWA // . VIII 2019. 158, 2. 84.

Garsden H., Greenhill L., Bernardi G., Fialkov A., Price D. C., Mitchell D., Dowell J., Spinelli M., Schinzel F. K. A 21-cm power spectrum at 48 MHz, using the Owens Valley Long Wavelength Array // . X 2021. 506, 4. 5802–5817.

Hallinan Gregg, Anderson Marin, Isella Andrea, Gary Dale, Bowman Judd, Romero-Wolf Andrew, OVRO-LWA Collaboration . The OVRO-LWA array — upgraded for real-time continuous all-sky imaging from 12-85 MHz // American Astronomical Society Meeting Abstracts. 241. I 2023. 451.09. (American Astronomical Society Meeting Abstracts).

Kern Nicholas S., Parsons Aaron R., Dillon Joshua S., Lanman Adam E., Fagnoni Nicolas, de Lera Acedo Eloy. Mitigating Internal Instrument Coupling for 21 cm Cosmology. I. Temporal and Spectral Modeling in Simulations // . X 2019. 884, 2. 105.

Kolopanis Matthew, Pober Jonathan C., Jacobs Daniel C., McGraw Samantha. New EoR power spectrum limits from MWA Phase II using the delay spectrum method and novel systematic rejection // Monthly Notices of the Royal Astronomical Society. VI 2023. 521, 4. 5120–5138.

O'Hara Oscar S. D., Dulwich Fred, de Lera Acedo Eloy, Dhandha Jiten, Gessey-Jones Thomas, Anstey Dominic, Fialkov Anastasia. Understanding spectral artefacts in SKA-Low 21-cm cosmology experiments: the impact of cable reflections // . IX 2024. 533, 3. 2876–2892.

Pober Jonathan C., Parsons Aaron R., Aguirre James E., Ali Zaki, Bradley Richard F., Carilli Chris L., DeBoer Dave, Dexter Matthew, Gugliucci Nicole E., Jacobs Daniel C., Klima Patricia J., MacMahon Dave, Manley Jason, Moore David F., Stefan Irina I., Walbrugh William P. Opening the 21 cm Epoch of Reionization Window: Measurements of Foreground Isolation with PAPER // . V 2013. 768, 2. L36.

Price D C, Greenhill L J, Fialkov A, Bernardi G, Garsden H, Barsdell B R, Kocz J, Anderson M M, Bourke S A, Craig J, Dexter M R, Dowell J, Eastwood M W, Eftekhari T, Ellingson S W, Hallinan G, Hartman J M, Kimberk R, Lazio T Joseph W, Leiker S, MacMahon D, Monroe R, Schinzel F, Taylor G B, Tong E, Werthimer D, Woody D P. Design and characterization of the Large-aperture Experiment to Detect the Dark Age (LEDA) radiometer systems // Monthly Notices of the Royal Astronomical Society. 05 2018. 478, 3. 4193–4213.

Trott Cathryn M., Jordan C. H., Midgley S., Barry N., Greig B., Pindor B., Cook J. H., Sleap G., Tingay S. J., Ung D., Hancock P., Williams A., Bowman J., Byrne R., Chokshi A., Hazelton B. J., Hasegawa K., Jacobs D., Joseph R. C., Li W., Line J. L. B., Lynch C., McKinley B., Mitchell D. A., Morales M. F., Ouchi M., Pober J. C., Rahimi M., Takahashi K., Wayth R. B., Webster R. L., Wilensky M., Wyithe J. S. B., Yoshiura S., Zhang Z., Zheng Q. Deep multiredshift limits on Epoch of Reionization 21 cm power spectra from four seasons of Murchison Widefield Array observations // . IV 2020. 493, 4. 4711–4727.